Oxidation behavior of T91 steel in flowing oxygen-containing lead-bismuth eutectic at 500 °C

S. J. Tian, Z. Z. Jiang* and L. Luo

T91 is considered as a possible structural material for lead-bismuth eutectic (LBE) cooled reactors. However, one of the main issues is the compatibility of T91 with LBE. In this work, the corrosion tests of T91 were performed in flowing (1 m/s) oxygen-controlled LBE (1–3 × 10^{-6} wt% O) at 500 °C for up to 5000 h. The results show that a three-layer oxide scale forms at the interface of T91 and LBE, consisting of Fe_3O_4 (magnetite), Fe-Cr spinel and an internal oxidation zone (IOZ). The growth kinetics of the oxide scale follows a parabolic dependence ($\Delta x^2 = k_p t$). The rate constants (k_p) of Fe_3O_4, Fe-Cr spinel, and IOZ are 0.052, 0.040, and 0.0057 μm²/h, respectively. In addition, the growth model of the oxide scale is established under consideration of the exfoliation process. This model clarifies the growth direction of each oxide layer and the transformation of Fe-Cr spinel to magnetite.

1 Introduction

Accelerator-driven subcritical system (ADS) has been internationally considered as an effective technological solution for nuclear waste transmutation [1,2]. Chinese Academy of Sciences (CAS) had launched a project to develop ADS and lead-based reactor technology since 2011. China lead-based reactor (CLEAR) was selected as the reference reactor for the ADS. At the first stage of CLEAR, a 10 MW research reactor named as CLEAR-I was constructed and lead-bismuth eutectic (LBE) was chosen as the coolant, due to its excellent thermal-physical properties and high neutron economy [3]. In order to support the designs of CLEAR-I, Institute of Nuclear Energy Safety Technology (INEST) carried out a series of research works, including structural materials development and evaluation [4,5], liquid metal loop technology [6], subcritical system design [7,8], and advanced nuclear software development [9]. Among these projects, one of the main issues is the compatibility of the candidate structural materials with LBE, which is one of the lifetime-determining factors for the reactor components, due to the dissolution of steel constituents into LBE at elevated temperatures. Furthermore, the surface oxide scale may reduce the heat transfer capability of the component wall, which is especially important for fuel cladding and heat exchanger tubes.

As a mature structural material widely used in advanced power plants, ferritic/martensitic (F/M) steel T91 has been selected as one of the candidate materials for the fuel cladding, heat exchangers or other near-core internals for CLEAR, ELSY, XT-ADS, and EFIT [10–12]. In earlier research [10,13–19], a lot of studies have been done to get the general performance and the basic corrosion mechanisms of T91 in LBE. These studies showed that $C_O = 10^{-6}$ wt% is a suitable range of oxygen concentration in LBE that allows in situ formation of thin protective oxide scale on the surface of T91 steel, which can prevent steel matrix from suffering dissolution attack. In recent years, the oxidation kinetics of T91 has been investigated in flowing LBE with around 10^{-6} wt% of dissolved oxygen at 450 and 550 °C, respectively [20,21]. It was found through comparison that the growth kinetics dependences and mechanism of the oxide scale on the T91 surface were different at various temperatures, even under the same oxygen concentration and flowing velocity. At present, *Weisenburger* et al. [22] proposed an empirical parabolic dependence for oxide scale growth as function of time and temperature, based on a large number of reliable experiments on T91 in LBE containing 10^{-6} wt% of oxygen in the temperature range of 420–550 °C. The parabolic rate constant as function of temperature in its relation followed a linear dependence. Furthermore, *Zhang* [23] proposed a theoretical model, in which the oxide layer removal was considered. The *Zhang*'s model has been used to study the growth kinetics of the oxide layers without consideration of the IOZ layer. However, the parabolic rate constant as function of the reciprocal of temperature (1/T) followed an exponential dependence [23], which is different from that in the empirical

S. J. Tian
University of Science and Technology of China, Hefei 230027, (P.R. China)

S. J. Tian, Z. Z. Jiang, L. Luo
Key Laboratory of Neutronics and Radiation Safety, Institute of Nuclear Energy Safety Technology, Chinese Academy of Sciences, Hefei 230031, (P.R. China)
E-mail: zhizhong.jiang@fds.org.cn

Table 1. Chemical composition of T91 steel (wt%)

C	Si	Mn	P	S	Cr	Ni	Mo	Nb	N	V	Fe
0.099	0.20	0.44	0.015	0.0016	9.25	0.25	0.85	0.067	0.050	0.19	Bal.

parabolic dependence [22]. Therefore, there are still some contradictions between the empirical dependence and the theoretical model. Moreover, when they were used to predict the thicknesses of the oxide layers, large differences have been seen between the computation results and experimental data [23]. It is difficult to predict the growth of the oxide layers in LBE accurately based on the present empirical dependences and theoretical models, because the growth behavior of oxide layers is very complex, depending not only on the oxygen concentration and the temperature but also on other operation conditions such as the coolant flow velocity and the flow path geometry [23].

In order to investigate the corrosion characteristics and to obtain kinetic data of T91 steel oxidation that can provide the reference for the design of CLEAR-I, corrosion tests of T91 were performed in flowing LBE with dissolved oxygen concentration of $(1–3) \times 10^{-6}$ wt%. The determination of the temperature and the flow velocity was based on the conceptual designs of CLEAR-I (the maximum cladding temperature and the maximum LBE flowing velocity are nearly 500 °C and 0.78 m/s, respectively). Besides, on the basis of the experimental results, a growth model of the oxide scale was established under the consideration of the exfoliation process, which can clarify the growth direction of each oxide layer and the transformation process of Fe-Cr spinel to magnetite.

2 Experimental

2.1 Materials and specimen preparation

The investigated specimens were machined from hot-rolled plates, the according chemical composition is listed in Table 1. The steel was austenitized at 1050 °C for 25 min, air cooling followed, subsequently tempering at 770 °C for 75 min and air cooling once again.

Figure 1 shows the dimensions of the specimens. As shown in Fig. 1a, the specimens were fabricated into cylinders, whose diameter and height are 12 and 35 mm, respectively. Both ends of each specimen have an internal screw thread and an external screw thread (Fig. 1b), respectively, for combining a number of these specimens for the exposure experiment in the flowing LBE. The specimen surfaces were polished with a grinding machine and cleaned with acetone in an ultrasonic bath. Before exposing to LBE, the initial diameters of the specimens were measured along the length of the specimens in steps of 5 mm by the laser micrometer with a resolution of 0.13 μm. For each transverse circular cross-section of the specimens, 12 measurements were performed to obtain accurate outside diameter by rotating the specimens with an angle of 30 ° at every turn.

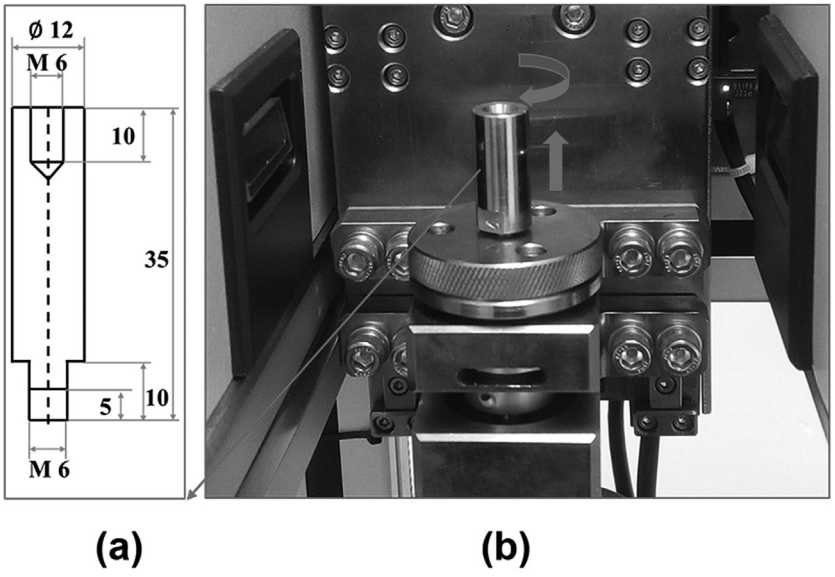

Figure 1. The dimensions of the specimens and the laser micrometer: (a) the schematic illustration of the cylindrical specimen and (b) the specimen in measurement

2.2 Test facility and test conditions

The test facility is a large scale-forced convection loop (named as KYLIN-II-M) for tests of long-term corrosion and oxygen control technology, as shown in Fig. 2, which was developed by the INEST•FDS team. The oxygen concentration in the flowing LBE was controlled via a gas phase oxygen control system, and monitored by electrochemical oxygen sensors at different positions along the loop. The oxygen concentration was calculated from the output voltage of oxygen sensor by the following formula:

$$\log(C_O) = -3.2837 + 6949.8/T\text{-}10080 \times E/T \quad (1)$$

where C_O is the oxygen concentration in wt%; T is the temperature in Kelvin; E is the output voltage of oxygen sensor in Volt [21].

Figure 3 shows the calculated oxygen concentration as a function of the runtime and the actual exposure time of the T91 specimens. The beginning and end of each exposure in relation to the total runtime is indicated by the bars in the bottom part of the diagram. The corrosion tests were carried out in flowing (1 m/s) LBE at 500 °C with (1–3) $\times 10^{-6}$ wt% dissolved oxygen for 500, 1000, 2000, 3000, and 5000 h.

2.3 Post-test analysis

In order to obtain corrosion data about the material loss of the steel and the oxide scale itself, two specimens were used in the same exposure time. One was chosen for cross-section examinations without removing LBE to reveal the morphologies and the dimensional parameters of oxide layers, and the other was examined for the trend for the corrosion damages and the material losses after the adherent LBE and the oxide scale were removed in turn. The surface and cross-section examinations of the specimens were performed with field emission scanning electron microscope (FE-SEM, Zeiss, SIGMA) supplemented by qualitative energy-dispersive X-ray microanalysis (EDX).

Figure 2. The picture of KYLIN-II-M loop

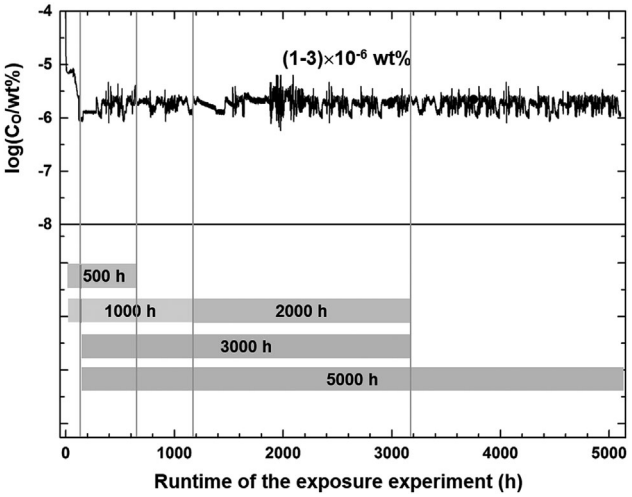

Figure 3. Calculated oxygen concentration as a function of the runtime and the actual exposure time of the T91 specimens

Chemical cleaning in a mixture solution of $CH_3COOH + H_2O_2 + C_2H_5OH$ with a volume ratio of 1:1:1 at room temperature was used to remove the adherent LBE on the surface of the specimens. The surface morphology and microstructure of the specimens after cleaning was examined by a camera and SEM, respectively. After the surface analysis, the oxide scale was removed by an alternate treatment with boiling alkaline $KMnO_4$ solution (pH = 12) and inhibited hydrochloric acid [24]. Subsequently, the diameter of the specimen matrix which was not affected by the LBE was determined with the same method as the measurement of the initial diameter by the laser micrometer. The material loss can be calculated by the following formula:

$$\Delta X_{ST} = 10^3 \times (D_0 - D_{ST})/2 = 500 \times (D_0 - D_{ST}) \quad (2)$$

where ΔX_{ST} is the material loss (μm); D_0 is the initial diameter of the specimen (mm); D_{ST} is the post-test diameter of the same specimen (mm). In all quantitative results, the confidence level of 95% was used due to the limited number of measurements.

3 Results and discussion

3.1 Corrosion characteristics

3.1.1 Microstructure of oxide scale

Figure 4 shows the typical cross-section morphologies of the oxide scales on the T91 specimen surfaces after different exposure times. It can be clearly seen that the oxide scales formed at the interface between the LBE and the matrix have similar structural features. The oxide scales have a three-layer structure: the outermost layer is a porous structure being penetrated by a small amount of LBE; the middle layer is more compact not exhibiting any LBE penetration; the innermost layer is a transitional zone. The results of EDX point analysis for the oxide scale shown in Fig. 4c are listed in Table 2. The outermost

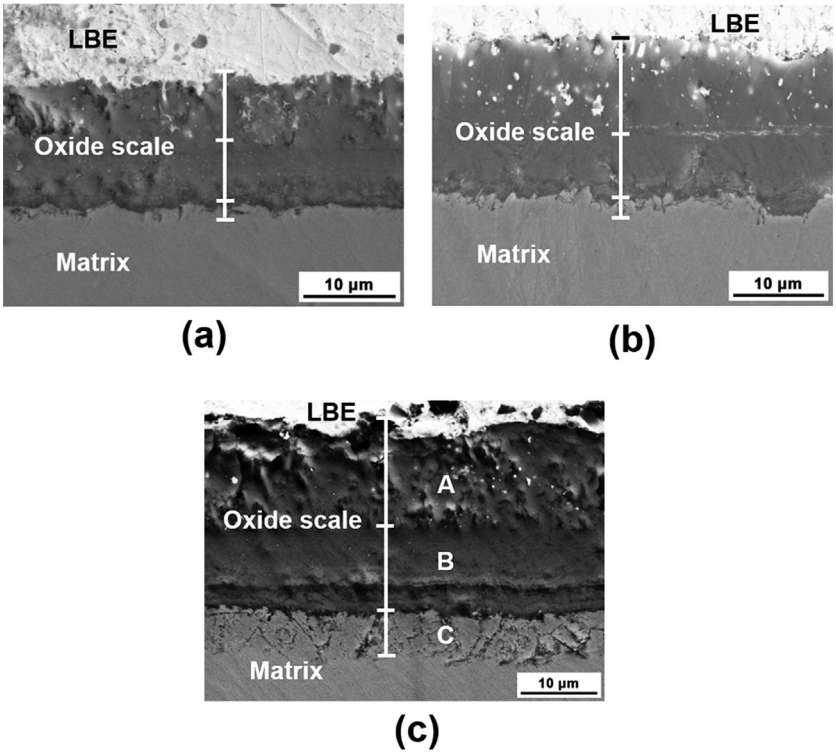

Figure 4. Typical cross-section morphologies of the oxide scales formed on the specimens after different exposure times: (a) 500 h, (b) 2000 h, and (c) 5000 h

layer mainly consists of Fe and O and the atomic ratio of Fe to O is 2.92:4, which indicates that the porous layer is magnetite (Fe_3O_4). The middle layer mainly consists of Fe, Cr, and O, and the atomic ratio of Fe + Cr to O is 2.88:4, which indicates that the impact layer is Fe-Cr spinel ($Fe_{3-x}Cr_xO_4$). The Fe-Cr spinel stoichiometry is $Fe_{2.4}Cr_{0.6}O_4$ according to the atomic ratio of Fe, Cr, and O, which is consistent with the results given in Ref. [18]. The innermost layer mainly consists of Fe, Cr, and a small amount of O, which is commonly known as an internal oxidation zone (IOZ). The chemical compositions of the other oxide scales after different exposure times were also determined by EDX point analysis and the results were essentially consistent. Hence, the whole oxide layers from exterior to interior are Fe_3O_4, $Fe_{2.4}Cr_{0.6}O_4$, and IOZ, respectively. The oxide scale structure is different from the results given in the report of *Zhang* who stated that IOZ layer was formed at temperatures equal or above 550 °C [23].

Table 2. Results of EDX quantitative analysis for the oxide scale shown in Fig. 4c

	Composition (at%)				
Position	Fe	O	Cr	Si	Mo
A	41.7	57.6	0.7	–	–
B	32.5	57.6	8.9	0.5	0.5
C	67.7	22.6	9.0	0.5	0.2

Figure 5 shows the results of the EDX line scan across the cross-section of the T91 specimen after exposure for 5000 h. The O content is very high in the magnetite and spinel layers but reduces rapidly in the IOZ layer along the direction of the matrix. The Fe content across the entire oxide layer is also very high, but it is slightly lower than that of the matrix. Compared with the other two oxide layers, the spinel layer has a lower Fe content. The Cr content in the IOZ and spinel layers is close to that in the matrix, but the average Cr content of the magnetite layer is very low. In addition, it is worth mentioning that Cr is locally enriched in some distance from the magnetite/spinel interface. The diffusion behavior of Fe, Cr, and O in Fig. 5b can be described by the "available space model" [16,18]. The Cr diffusion is negligible in comparison with Fe, because the Cr self-diffusion coefficient in Fe-Cr spinel is approximately three orders of magnitude lower than that of the Fe [25]. Hence, after a very thin spinel layer is formed on the surface of the steel, Fe from the spinel at firstly diffuses to the surface being oxidized and forming the magnetite layer. The outward diffusion of Fe resulted in some vacancy accumulations in the Fe-Cr steel [16]. Then, these vacancies can segregate at the steel/oxide interface to form micro-cavities [16]. These cavities were filled with the Fe-Cr spinel formed by reaction of Fe and Cr with the inwards diffusing O. The outward diffusion of Fe in the Fe-Cr spinel resulted in a concentration gradient of Fe between the spinel and the matrix. Hence, the Fe in the matrix surface region could diffuse outwards, which results in the decrease of the Fe content. For the same reason, the O could diffuse inwards and reacts with the Cr in the matrix surface region. The mutual diffusion of Fe and O at the

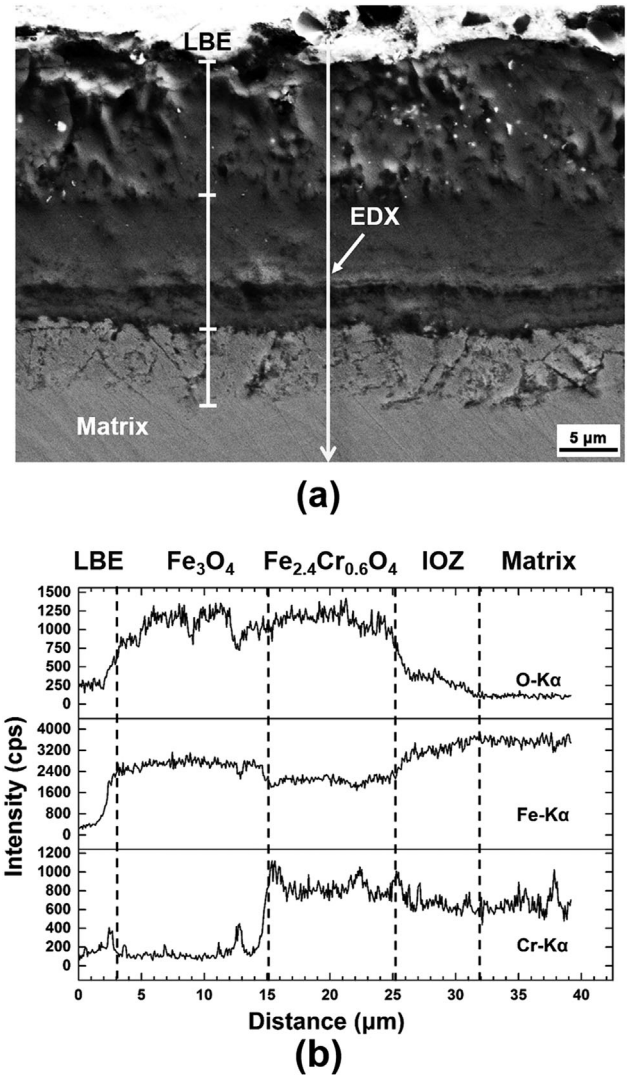

Figure 5. Results of the EDX line scan through the cross-section of the specimen after exposure for 5000 h: (a) the cross-section morphology and (b) the results of the EDX line scan

spinel/matrix interface resulted in the formation of the IOZ layer. Consequently, the mutual diffusion of Fe, Cr, and O at the LBE/matrix interface causes the formation of the oxide scale with its three-layer structure.

3.1.2 The exfoliation of oxide scale

Figure 6 shows general and detailed surface appearance of the specimens after exposure in LBE for different exposure times. As shown in Fig. 6a, the initial surface has a metallic luster with visible polishing grooves. After exposure for 500 h, the major part of the specimen surface is covered and protected by a black-colored oxide scale (Fig. 6b). Some white-colored zones represent the exfoliation of oxide scale. With the increase of exposure time, more and more white-colored zones appear on the surface (Fig. 6c and d). This indicates that the local exfoliation degree of oxide scale becomes worse with the increase of exposure time. As shown in detail view of Fig. 6d, the exfoliation of the oxide scale is directly observed on a local surface of the specimen exposed to the LBE for 5000 h. The exfoliation of the oxide scale may be caused by the erosion of the flowing LBE [26].

To reveal the exfoliation process of oxide scale, a set of detailed surface examinations on the oxide scale exfoliation zones in Fig. 6b–d was performed and the results are summarized in Figs. 7–9. As shown in Fig. 7, the surface morphologies of the regions A and B are different: the A-region exhibits a porous structure with many micro-cavities, while the B-region reveals a compact structure with some grooves on the surface. The results of EDX point analysis on regions A and B are listed in Table 3. The atomic ratios of Fe and (Fe + Cr) to O are 2.88:4 and 2.92:4, respectively, indicating that the A-region is Fe_3O_4 and the B-region is Fe-Cr spinel. By comparing with Fig. 6a, it is concluded that the grooves on the B-region are the residual traces resulting from the mechanical polishing. Hence, it can be deduced that the Fe-Cr spinel layer grows into the steel matrix while the magnetite layer grows into LBE at the magnetite/liquid metal interface. This is also supported by the ^{18}O tracer oxidation experiments of T91 [16]. In conclusion, the outermost layer Fe_3O_4 locally started to flake off at the early stage of corrosion.

After exposure for 2000 h, the exfoliation degree of the oxide scale becomes worse. Figure 8 shows a crater observed in the exfoliation regions of the oxide scale. The Fe, Cr, and O maps of the area inside the frame show an absence of O but the enrichment of Cr and Fe at the bottom of the crater and the enrichment of Cr and O on the small platform (region C). The EDX point analysis for these two different regions was performed too and the results are listed in Table 4. These results reveal that the C-region on the small platform is Fe-Cr spinel and the composition on the D-region is similar to the original composition of the T91 steel matrix. Besides, a small amount of O was found at the bottom. It can be concluded that the formation of the crater is a result of the exfoliation process of Fe_3O_4, Fe-Cr spinel, and IOZ. In the end, slight in situ oxidation occurred at the bottom.

Figure 9 shows a larger exfoliation region observed on the specimen surface after exposure for 5000 h and the according EDX mapping analysis for the whole region. The composition of the irregular exfoliation region mainly consists of Fe and O; the composition along its edge is Fe, Cr, and O; while the composition around the exfoliation region consists of Fe and O. The oxide layer of the E-region has a porous structure while the morphology of the G-region is similar to the martensitic microstructure of the matrix. The results of EDX point analysis of regions E–G in Fig. 9 are listed in Table 5. Table 5 indicates that the E-region consists of Fe_3O_4, the composition of the F-region at the edge of the irregular region is close to Fe-Cr spinel and in the G-region approximates Fe_3O_4. It can be concluded that the steel matrix was oxidized in situ again after exfoliation happened at the whole oxide scale.

Based on the above analysis, the exfoliation process of oxide scale can be described as follows: (1) the outermost layer (Fe_3O_4) locally starts to flake off at the early stage of corrosion. (2) With the increase of exposure time, the local exfoliation of both the Fe-Cr spinel and IOZ occurs. (3) The exfoliation region of the oxide scale becomes larger with the increase of exposure time. (4) The exfoliation region can be re-oxidized in situ again. This can

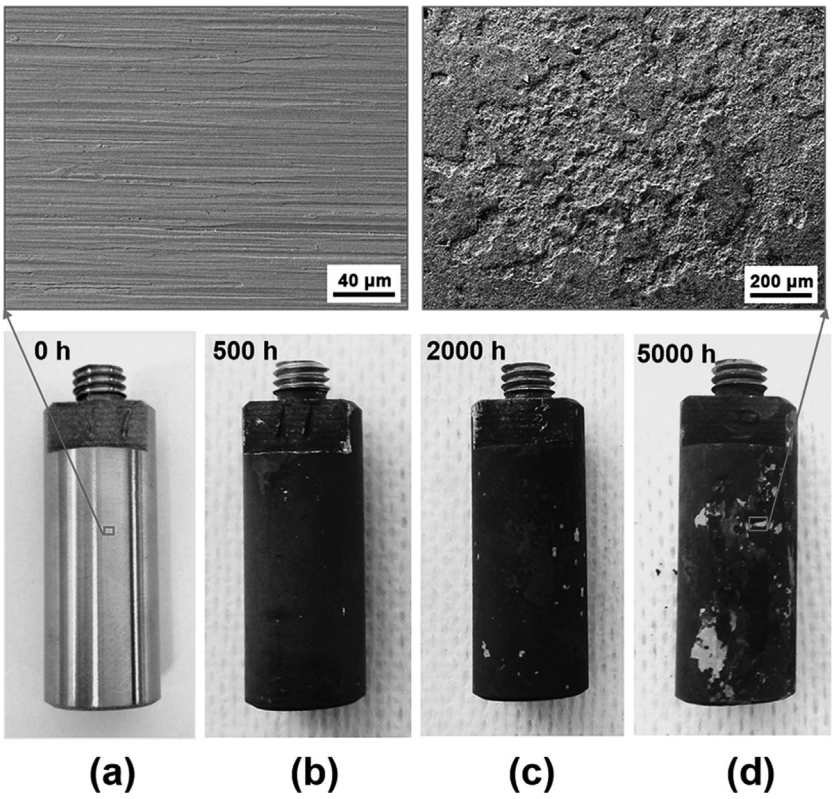

Figure 6. General and detailed surface appearance of the specimens after machining and exposure to the flowing LBE: (a) 0 h, (b) 500 h, (c) 2000 h, and (d) 5000 h

be helpful to prevent further penetration of LBE into the steel matrix.

3.2 Oxidation kinetics

3.2.1 The growth kinetics of the oxide scale

Figure 10 shows the experimental values and the corresponding fitted curves for the thickness of oxide scale. The total thickness of the magnetite plus spinel layer has an important effect on the reduction of the heat transfer capability of the component wall. In the case of the spinel plus IOZ layer, the total thickness contributes to reduce the mechanical stability of the component. The thickness of the oxide scale shows an overall increase trend as a function of time. After 5000 h, the average thickness of magnetite plus spinel plus IOZ is around 33 μm and the average thickness of spinel plus IOZ is about 18 μm. The quantitative data obtained for the thickness of the oxide layers can be analyzed by means of the appropriate kinetic dependences. According to the variation tendency of the oxide layer thickness with time shown in Fig. 10, the oxidation of the T91 in the LBE was fitted

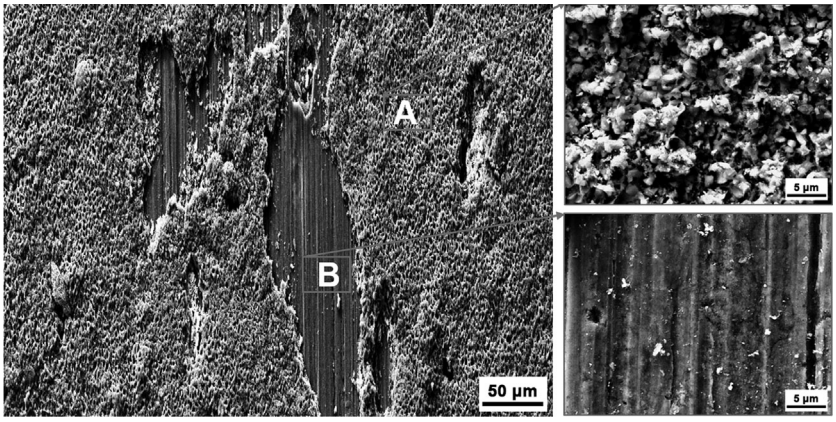

Figure 7. Surface morphology for the specimen after exposure for 500 h: the A-region is Fe_3O_4 and the B-region is Fe-Cr spinel

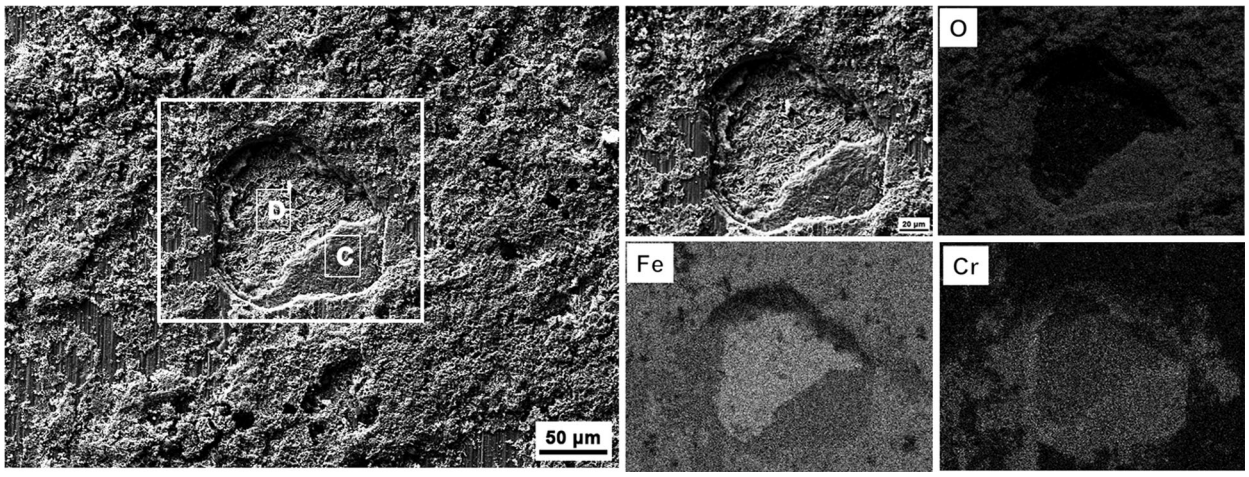

Figure 8. Morphology and results of EDX mapping analysis for the crater observed on the specimen surface after exposure for 2000 h

using the logarithmic dependence and the parabolic dependence, respectively. It was found that the parabolic rule seems to be more accurate to describe the average thickness dependence of the oxide layers. Therefore, the experimental values in Fig. 10 are fitted with the following parabolic equation:

$$\Delta x^2 = k_p t \tag{3}$$

where Δx is the thickness of the oxide scale (μm), k_p is the rate constant ($\mu m^2/h$) and t is the exposure time (h). The k_p values of magnetite, spinel, and IOZ layers are 0.052, 0.040, and 0.0057 $\mu m^2/h$, respectively. The k_p values of IOZ plus spinel, magnetite plus spinel, and the whole oxide scale are 0.072, 0.18, and 0.24 $\mu m^2/h$, respectively. According to the extrapolation of the parabolic law, the average thickness of the whole oxide scale after exposure for 1 year is about 46 μm.

Table 6 shows the comparison results of the parabolic rate constants for the T91 steel in LBE with around 10^{-6} wt% dissolved oxygen at different temperatures and velocities [10,20–23]. The experimental k_p at 500 °C and 1 m/s are different from that at other temperatures and velocities. According to the empirical dependence given by *Weisenburger* et al. [22], the calculated k_p of the whole oxide scale at 500 °C is 0.084 $\mu m^2/h$, but the k_p value of each oxide layer cannot be calculated. Furthermore, based on the *Zhang*'s theoretical model considering the erosive removal of oxide layers [23], the calculated k_p of the spinel layer at 500 °C should be 0.16 $\mu m^2/h$. The k_p value of the magnetite and IOZ layers cannot be

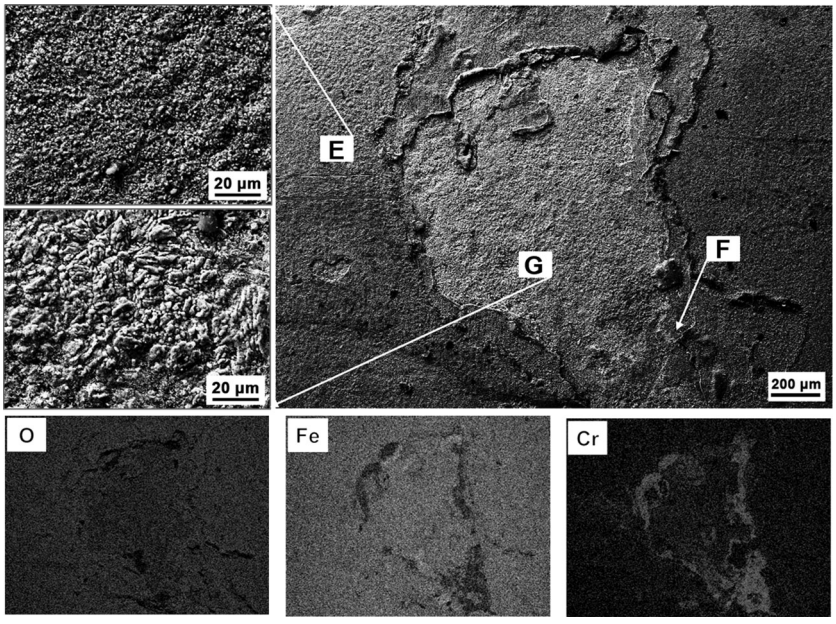

Figure 9. Morphology of the larger exfoliation region observed on the specimen surface after exposure for 5000 h and results of EDX mapping analysis for the whole region

Table 3. Results of EDX point analysis of regions A and B in Fig. 7

	Composition (at%)				
Position	Fe	O	Cr	Si	Mo
A	41.6	57.8	0.6	–	–
B	31.1	57.3	10.7	0.5	0.4

Table 5. Results of EDX point analysis of regions E–G in Fig. 9

	Composition (at%)			
Position	Fe	O	Cr	Si
E	41.1	57.2	1.6	–
F	23.6	58.2	17.2	1.0
G	42.0	54.6	3.4	–

calculated, because the dissolution rate or the removal rate of magnetite is unknown and the IOZ layer growth cannot be predicted by the model so far. It was found through comparison that the experimental k_p at 500 °C also exhibit large differences from the calculated values. The main differences of the k_p values listed in Table 6 and the corresponding explanations are as follows:

(1) It is well-known that the diffusion coefficients are a function of temperature and the increase of temperature results in higher elements diffusion coefficients [27]. According to the *Weisenburger*'s empirical dependence [22] and the *Zhang*'s theoretical model [23], the k_p value of the oxide layer has a positive correlation with temperature. As a result, under the condition of the flow velocity of 1 m/s, the k_p values at 550 °C are higher than that at 500 °C, except for that of the magnetite layer at 550 °C, which may be because the magnetite layer partly flaked off or was dissolved at higher temperatures. In the case of 2 m/s, the k_p value of the spinel layer at 550 °C is higher than that at 450 °C.

(2) Russian experience indicates that the oxygen concentration and flow velocity are the two most important factors affecting the oxide layer growth [23]. In a flowing non-isothermal loop, corrosion products can be transported by both diffusion and convection [27]. At low velocities (less than 2 m/s^{-1}), oxidation is controlled or partially controlled by mass transfer and the concentrations of corrosion products at the interface of the steel and LBE equal to the saturation or equilibrium [27]. Therefore, the thickness of the laminar mass transfer layer becomes thinner with increasing the flow velocity. In this case, increasing the flow velocity leads to a higher concentration gradient of alloy compositions between the matrix and the LBE, which results in higher diffusion coefficients of the elements. Therefore, the increase of the flow velocity causes higher growth rates and the according parabolic rate constants for the oxide layers. However, when the flow velocities in loops are more than 2 m/s^{-1}, the magnetite layer is removed by the flowing LBE [26]. Hence, under the condition of 550 °C, the k_p value of the spinel layer at 2 m/s^{-1} is much higher than that at 1 m/s^{-1} and the magnetite layer at 2 m/s^{-1} was missing probably due to the erosion of the LBE.

(3) It is crucial and very interesting to model the long-term behavior to predict materials lifetime in LBE. The previous

Table 4. Results of EDX point analysis of regions C and D in Fig. 8

	Composition (at%)				
Position	Fe	O	Cr	Si	Mo
C	30.6	57.7	10.8	0.5	0.5
D	79.5	9.0	11.1	0.3	0.2

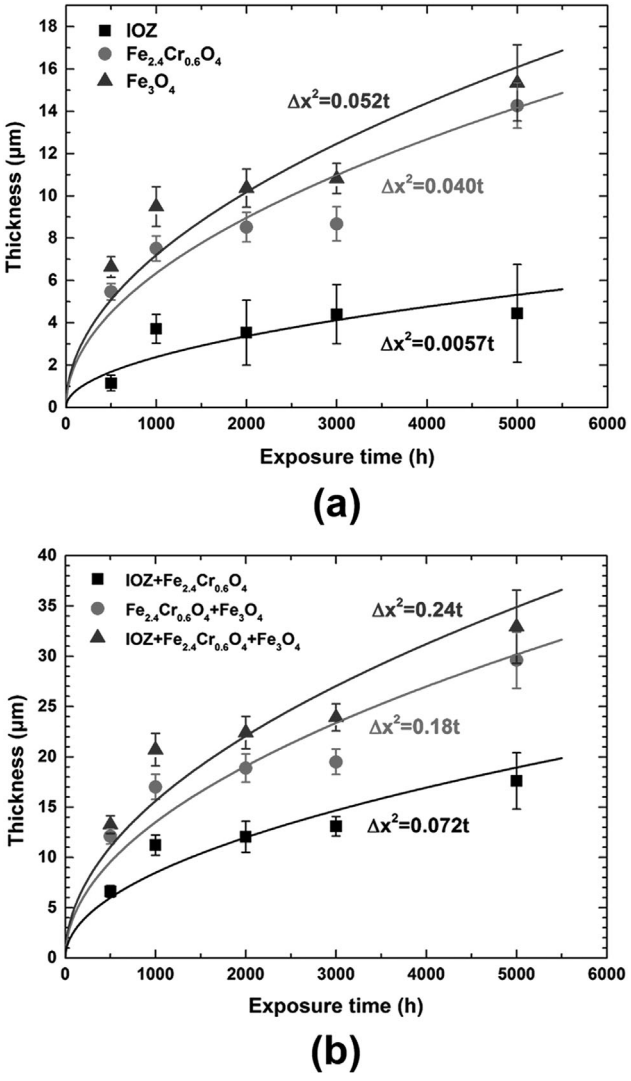

Figure 10. Experimental values and the engineering 1D curves fitting the measured data points: (a) the growth dependence of each oxide layer and (b) the growth dependence of the relevant layers

Table 6. Comparison of the parabolic rate constants for the T91 steel in flowing LBE with around 10^{-6} wt% dissolved oxygen at different temperatures and flow velocities

Oxide layers	K_p ($\mu m^2/h$)					
	450 °C 2 m/s [20]	500 °C 1 m/s	500 °C *Zhang*'s model [23]	500 °C *Weisenburger*'s empirical dependence [22]	550 °C 1 m/s [10]	550 °C 2 m/s [21]
Magnetite	0.025	0.052	–	–	0.048	missing
Spinel	0.013	0.040	0.16	–	0.048	0.20
IOZ	0	0.0057	–	–	0.026	–
Magnetite + spinel	0.074	0.18	–	–	0.25	0.20
Oxide scale	0.074	0.24	–	0.084	0.44	–

experimental results have indicated that the oxidation constant and the corrosion rate are functions of the temperature, flow velocity, oxygen concentration, steel composition, and the temperature difference [26]. It is still impossible to establish any correlations to predict accurately the growth of the oxide layers. Therefore, the experimental k_p values are largely different from the calculated values.

3.2.2 *The position evolution dependences of interfaces and the surfaces of the oxide layers*

To clarify the growth direction of each oxide layer and the transformation dependences of Fe-Cr spinel to magnetite, the evolution dependences of the instantaneous positions of the interfaces and surface of the oxide layers with time were studied, as shown in Fig. 11. The detailed calculation methods of the instantaneous position are given in Appendix A. As shown in Fig. 3, the oxygen concentration in the LBE was at its saturated value in the initial phase of the loop running. It needs about 100 h to reach the final oxygen concentration, resulting in that the 500 and 1000 h specimens put into the loop at the early stage were over oxidized. Hence, the experimental data for the first 1000 h are not precise enough (statistically). The following discussion will ignore these discrete points. As shown in Fig. 11, X_M is greater than zero and moves in the positive direction while X_{IOZ} is the opposite of X_M all the time at the first 5000 h. This implies that the magnetite layer grows outwards and the spinel layer grows inwards, confirming the results of the surface analysis for the specimen after exposure for 500 h (see Section 3.1.2). The movement of the magnetite/spinel interface with time is determined by X_{SP}, indicating that the interface position moves in the direction of the spinel growth, position starting from the initial state of the steel surface. This implies that a solid-state transformation of spinel to magnetite may occur. If the solid-state transformation is not completed thoroughly, the local Cr enrichment can be observed inside the magnetite layer occasionally (Fig. 5b).

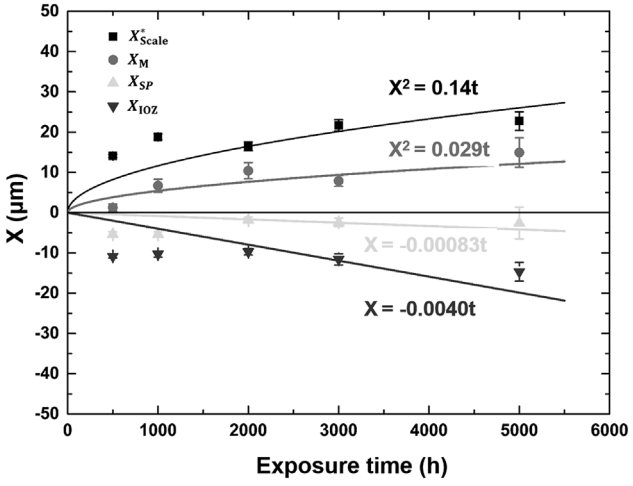

Figure 11. The position evolution dependences for interfaces and oxide layers surfaces with time. X^*_{Scale} is the instantaneous position of the scale surface assuming that no dissolution of steel constituents into the LBE or any other degradation of the scale occurred. X_M, X_{SP}, and X_{IOZ} correspond to the instantaneous position of the interface between magnetite and LBE, the interface between magnetite and the Fe-Cr spinel, and the interface between IOZ and the matrix, respectively

As shown in Fig. 11, it may be reasonable that a linear dependence is used to fit the position evolution of X_{SP} and X_{IOZ} while a parabolic dependence is used to fit the position evolution of X_M and X^*_{Scale}. The parabolic rate constants of X_M and X^*_{Scale} are 0.029 and 0.14 $\mu m^2/h$, respectively. The position of X^*_{Scale} is always on the top of X_M, implying that the diffusion of steel constituents from the solid phases to the LBE or/and the exfoliation of the oxide scale have occurred. The amount of metal dissolution per unit area can be obtained from $(X^*_{Scale} - X_M) \times \rho_{Me;\ Scale}$. Hence, the dissolution flux of metals into LBE, j_{metal} ($mg\,m^{-2}\,h^{-1}$), is given by the following relation:

$$j_{metal} = \rho_{Me;\ Scale} \frac{d}{dt}(X^*_{Scale} - X_M) = \frac{367}{\sqrt{t}} \quad (4)$$

where j_{metal} is the amount of metal dissolution into LBE per unit surface area and per unit time ($mg\,m^{-2}\,h^{-1}$); $\rho_{Me;\ Scale}$ is the average partial density of metals in the oxide scale, which is identified with the partial density of Fe in magnetite (3.7 g/cm^3). From Equation (4), j_{metal} decreases with the increase of time. By the calculation from Equation (4), $j_{metal} < 26.0\,mg\,m^{-2}\,h^{-1}$ after 200 h, $<11.6\,mg\,m^{-2}\,h^{-1}$ after 1000 h and $<5.2\,mg\,m^{-2}\,h^{-1}$ after 5000 h. *Schroer* et al. [21] have investigated the corrosion behavior

of T91 in oxygen-containing LBE (550 °C, 2 m/s and 1.6×10^{-6} wt%) in the CORRIDA loop, $j_{metal} < 70\,mg\,m^{-2}\,h^{-1}$ after 200 h, and $<20\,mg\,m^{-2}\,h^{-1}$ after 1000 h. Comparing with these results of *Schroer* et al., the values for j_{metal} under the present test conditions are much smaller due to the lower temperature and flow rate, which is beneficial for the protection of structure materials. According to the linear dependence of X_{SP} with time, the rate of the solid-state transformation of spinel to magnetite is approximately equal to 8×10^{-4} μm/h, indicating that the solid-state transformation rate is very slow. Such a low rate is good for the protection of the structure materials because the outer magnetite layer owning a porous structure is less protective than the inner spinel layer [23]. Furthermore, based on the linear dependence of X_{IOZ} with time, the movement rate of the IOZ/spinel interface in the direction of the matrix is roughly equal to 4×10^{-3} μm/h. This implies that the transformation of IOZ to spinel is also in existence and the faster transformation rate is beneficial for the rapid growth of the spinel layer.

3.3 The growth model of oxide scale

Based on the analysis of the Sections 3.1 and 3.2 and the previous literature [16,18,20], the growth model of the oxide scale under the test conditions is established in combination with its exfoliation process of oxide scale. Besides the exfoliation process of oxide scale, the elemental diffusion mechanism at the interface between the matrix and LBE, the growth direction of each oxide layer and the transformation process of Fe-Cr spinel to magnetite are systematically considered in the growth model. The growth process is divided into the following four stages and a schematic illustration is shown in Fig. 12. (1) When the T91 is exposed to the LBE, a small quantity of Ni, Fe, and Cr near the steel surface dissolve into LBE and then the removal of these elements creates vacancy clusters in the steel matrix. The O in LBE diffuses into these vacancy clusters and reacts with Fe and Cr. A very thin spinel layer is formed on the surface of the steel (Fig. 12a). (2) Fe from the steel matrix diffuses easily throughout the thin spinel layer and reacts with O to form the magnetite layer that grows outwards at the interface of magnetite and LBE. Meanwhile, the Fe-Cr spinel grows inwards at the interface of the matrix and Fe-Cr spinel by the reaction of Fe and Cr with the inwards diffusing O. At the early stage of corrosion, the magnetite layer locally starts to flake off (Fig. 12b). (3) The oxide scale continues to grow by elemental diffusion. However, with the increase of exposure time, the local exfoliation of the Fe-Cr spinel and IOZ layers occurs (Fig. 12c). (4) The position of the magnetite/spinel interface moves in the direction of the spinel growth, position starting from the original place to the steel surface, indicating that a solid-state transformation of spinel to magnetite has occurred. The exfoliation region of the oxide scale becomes larger with time, meanwhile, the exfoliation region can be oxidized in situ again (Fig. 12d). It can be deduced that the exfoliation and regeneration of the oxide scale can occur circularly.

4 Conclusions

In the present study, the oxidation behaviors of the T91 in flowing oxygen-containing LBE at 500 °C, 1 m/s and $1–3 \times 10^{-6}$ wt% for up to 5000 h have been investigated. The main conclusions are as follows:

(1) An oxide scale with a typical three-layer structure formed at the interface between LBE and the matrix. The whole oxide layers from exterior to interior are Fe_3O_4, $Fe_{2.4}Cr_{0.6}O_4$, and

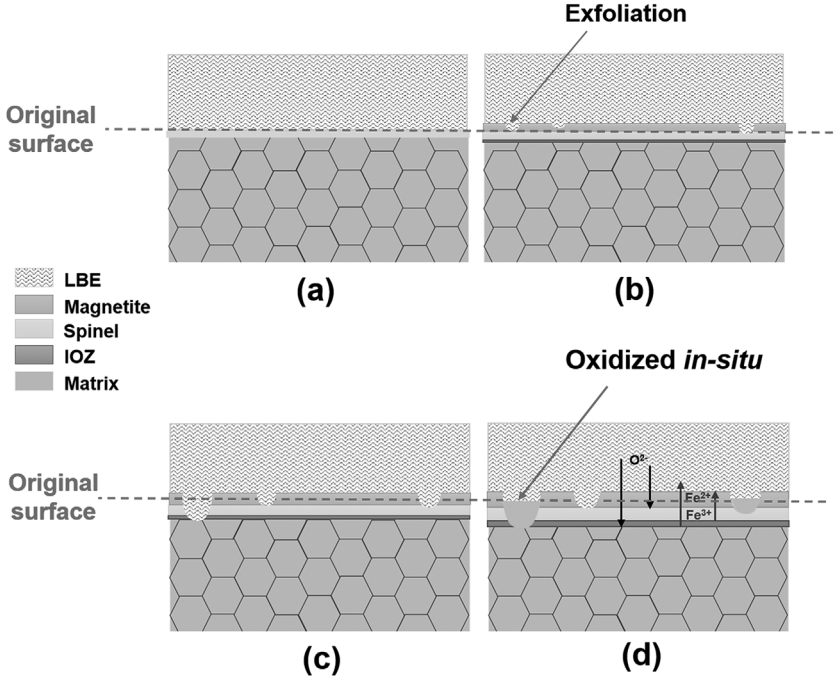

Figure 12. The oxide scale growth model on the surface of T91 specimens

IOZ respectively, which is different from the summary of *Zhang*. The growth kinetics of each layer follows a parabolic law. The k_p values for Fe_3O_4, $Fe_{2.4}Cr_{0.6}O_4$, and IOZ layers are 0.052, 0.040, and 0.0057 $\mu m^2/h$, respectively. The k_p values for IOZ plus spinel, magnetite plus spinel, and the total scale thickness are 0.072, 0.18, and 0.24 $\mu m^2/h$, respectively.

(2) The parabolic rate constants change with temperature and flow velocity even under the same oxygen concentration and a positive correlation with them was in existence in a limited range. From the perspective of the oxide scale growth and metal dissolution, it is beneficial for the protection of key materials to reduce the operating temperature and flow velocity.

(3) The growth model of the oxide scale is established in combination with the exfoliation process of oxide scale: (a) the magnetite layer that grows outwards at the magnetite/LBE interface, while the Fe-Cr spinel grows inwards at the matrix/Fe-Cr spinel interface. Meanwhile, the solid-state transformation of spinel to magnetite has occurred at the magnetite/Fe-Cr spinel interface; (b) the outermost oxide layer (Fe_3O_4) flakes off at some local regions. Subsequently, the Fe-Cr spinel and IOZ layers start to crack and flake off, too. The exfoliation region of the oxide scale becomes lager with time and can be oxidized in situ again.

Acknowledgments: This work is supported by the National Natural Science Foundation of China (nos. 51401204 and 51501185), the Natural Science Foundation of Anhui Province of China (1508085QE108), and the Strategic Priority Research Program of Chinese Academy of Sciences (no. XDA03040000). We would like to thank for the great help we got from Dr. *Zhang Min* and other members of the FDS team in this research.

Appendix A. The detailed calculation methods of the instantaneous positions of the interfaces and surfaces of the oxide layers [20].

Figure A13 shows the schematic illustration of the corrosion interface of Cr-containing steels in liquid Pb-alloys with oxygen, which has been used by *Schroer* et al. [20]. The capital X with different indices for the steel (ST) and the oxide layers forming on the steel surface denotes the instantaneous position of interfaces and surface of the oxide layers, respectively. M, SP, IOZ, and DZ correspond to magnetite, Fe-Cr spinel, an internal oxidation zone and another depleted zone inside the steel, respectively. The positive direction of X-axis points from the initial position of the steel surface towards outside (LBE). X_0 is the initial position of the steel surface and X^*_{Scale} is the instantaneous position of the scale surface on the assumption that no dissolution of steel constituents into the LBE or any other degradation of the scale occurred. The instantaneous thickness of the oxide layers (ΔX with respective index) is the difference between the positions of the terminating interfaces. It need to be specially mentioned that ΔX_{d} is the part of oxide scale lost to the liquid–metal environment and can be determined from a mass balance between the consumed steel and the amount of metal retained in the observed oxide scale. Moreover, the material loss, ΔX_{ST}, represents the difference between X_0 and X_{ST}. The IOZ layer is included in the corrosion loss, because it has less good mechanical properties in comparison to the unaffected material. The depletion zone is naturally a part of the remaining matrix, but, depending on the degree of the depletion of specific steel constituents, it may have to be added to ΔX_{ST}, in order to quantify the whole material degradation accurately. It should be noted that the magnetite layer, IOZ or DZ, may be missing in particular cases. Hence, sometimes the schematic illustration shown in Fig. A1 requires some slight modifications.

It is worth mentioning that ΔX_{DZ} equals to zero and the thickness of IOZ (ΔX_{IOZ}) is not neglected in the present study. The reasons are as follows: (1) the depletion of the steel constituents in the steel matrix is not significant according to the EDX line scan results of scales in Fig. 5b; (2) the IOZ layer is highly visible and cannot be ignored. Considering that the content of alloy elements in the IOZ layer is in close proximity to that in the matrix, ΔX_{d} is given by

$$\Delta X_{\mathrm{d}} = \rho_{\mathrm{ST}}/\rho_{\mathrm{Me;\ Scale}} \times (\Delta X_{\mathrm{ST}} - \Delta X_{\mathrm{IOZ}}) - (\Delta X_{\mathrm{M}} + \Delta X_{\mathrm{SP}}) \quad \text{(A1)}$$

where ρ_{ST} denotes the density of the steel (7.7 g/cm for T91) and $\rho_{\mathrm{Me;\ Scale}}$ is the average partial density of metals in the oxide scale,

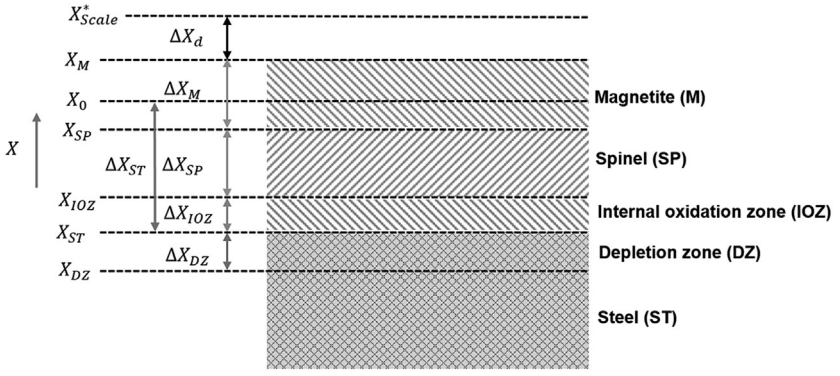

Figure A13. Schematic illustration of the corrosion interfaces: Cr-containing steels in liquid Pb-alloys with oxygen [20]

which is identified with the partial density of Fe in magnetite (3.7 g/cm).

If the quantitative data for ΔX_M, ΔX_{SP}, ΔX_{IOZ}, ΔX_{ST}, and ΔX_d have been obtained, the instantaneous positions of the interfaces and surface of the oxide layers (X^*_{Scale}, X_M, X_{SP}, and X_{IOZ}) will be deduced from the following relations:

$$X_0 - X_{SP} = \Delta X_{ST} - \Delta X_{SP} - \Delta X_{IOZ} \quad \text{(A2)}$$

$$X^*_{Scale} = \Delta X_M + X_{SP} + \Delta X_d \quad \text{(A3)}$$

$$X_M = \Delta X_M + X_{SP} \quad \text{(A4)}$$

$$X_{IOZ} = \Delta X_{IOZ} - \Delta X_{ST} \quad \text{(A5)}$$

5 References

[1] E. Greenspan, P. Hejzlar, H. Sekimoto, G. Toshinsky, D. Wade, *Nucl. Technol.* **2005**, *151*, 177.
[2] Z. Chen, Y. Wu, B. Yuan, D. Pan, *Ann. Nucl. Energy* **2015**, *75*, 723.
[3] Y. Wu, Y. Bai, Y. Song, Q. Huang, Z. Zhao, L. Hu, *Ann. Nucl. Energy* **2016**, *87*, 511.
[4] Q. Huang, FDS Team, *J. Nucl. Mater.* **2014**, *455*, 649.
[5] Q. Huang, Y. Wu, J. Li, F. Wan, J. Chen, G. Luo, X. Liu, J. Chen, Z. Xu, X. Zhou, *J. Nucl. Mater.* **2009**, *386*, 400.
[6] Y. Wu, Q. Huang, Z. Zhu, S. Gao, Y. Song, *Fusion Sci. Technol.* **2012**, *62*, 272.
[7] Y. Wu, J. Jiang, M. Wang, M. Jin, FDS Team, *Nucl. Fusion* **2011**, *51*, 103036.
[8] Y. Wu, FDS Team, *Fusion Eng. Des.* **2006**, *81*, 2713.
[9] Y. Wu, J. Song, H. Zheng, G. Sun, L. Hao, P. Long, L. Hu, FDS Team, *Ann. Nucl. Energy* **2015**, *82*, 161.
[10] A. Weisenburger, C. Schroer, A. Jianu, A. Heinzel, J. Konys, H. Steiner, G. Muller, C. Fazio, A. Gessi, S. Babayan, A. Kobzova, L. Martinelli, K. Ginestar, F. Balbaud-Celerier, F. J. Martin-Munoz, L. S. Crespo, *J. Nucl. Mater.* **2011**, *415*, 260.
[11] A. Alemberti, J. Carlsson, E. Malambu, A. Orden, D. Struwe, P. Agostini, S. Monti, *Nucl. Eng. Des.* **2011**, *241*, 3470.
[12] J. Liu, Z. Jiang, S. Tian, Q. Huang, Y. Liu, *J. Nucl. Mater.* **2016**, *468*, 299.
[13] C. Schroer, Z. Voss, O. Wedemeyer, J. Novotny, J. Konys, *J. Nucl. Mater.* **2006**, *356*, 189.
[14] D. Sapundjiev, S. Van Dyck, W. Bogaerts, *Corros. Sci.* **2006**, *48*, 577.
[15] O. Yeliseyeva, V. Tsisar, G. Benamati, *Corros. Sci.* **2008**, *50*, 1672.
[16] L. Martinelli, F. Balbaud-Celerier, A. Terlain, S. Delpech, G. Santarini, J. Favergeon, G. Moulin, M. Tabarant, G. Picard, *Corros. Sci.* **2008**, *50*, 2523.
[17] Y. Kurata, M. Futakawa, S. Saito, *J. Nucl. Mater.* **2008**, *373*, 164.
[18] L. Martinelli, F. Balbaud-Célérier, A. Terlain, S. Bosonnet, G. Picard, G. Santarini, *Corros. Sci.* **2008**, *50*, 2537.
[19] L. Martinelli, F. Balbaud-Celerier, G. Picard, G. Santarini, *Corros. Sci.* **2008**, *50*, 2549.
[20] C. Schroer, O. Wedemeyer, A. Skrypnik, J. Novotny, J. Konys, *J. Nucl. Mater.* **2012**, *431*, 105.
[21] C. Schroer, J. Konys, *J. Eng. Gas. Turb. Power* **2010**, *132*, 082901.
[22] A. Weisenburger, L. Mansani, G. Schumacher, G. Müller, *Nucl. Eng. Des.* **2014**, *273*, 584.
[23] J. S. Zhang, *Oxid. Met.* **2013**, *80*, 669.
[24] C. Schroer, Z. Voss, J. Novotny, J. Konys, *Quantification of the degradation of steels exposed to liquid lead-bismuth eutectic*, Report FZKA 7224, Karlsruhe, Germany **2006**.
[25] J. Töpfer, R. Dieckmann, *Solid State Ionics* **1995**, *81*, 251.
[26] C. Fazio, V. Sobolev, A. Aerts, S. Gavrilov, K. Lambrinou, P. Schuurmans, A. Gessi, P. Agostini, A. Ciampichetti, L. Martinelli, *Handbook on Lead-Bismuth Eutectic Alloy and Lead Properties, Materials Compatibility, Thermal-Hydraulics and Technologies*, OECD, Vienna, Austria **2015**.
[27] J. S. Zhang, N. Li, *J. Nucl. Mater.* **2008**, *373*, 351.

(Received: May 18, 2016) W9075
(Accepted: July 19, 2016)